molecular pharmaceutics

Article

pubs.acs.org/molecularpharmaceutics

# Restoring Basal Planes of Graphene Oxides for Highly Efficient Loading and Delivery of β-Lapachone

Xin Ting Zheng[†,‡] and Chang Ming Li*[,†,‡]

[†]Institute for Clean Energy and Advanced Materials, Southwest University, Chongqing 400715, P. R. China

[‡]School of Chemical and Biomedical Engineering, Center for Advanced Bionanosystems, Nanyang Technological University, 70 Nanyang Drive, Singapore 637457, Singapore

Supporting Information

**ABSTRACT:** An efficient and biocompatible drug nanocarrier is essential for nanomedicines to realize their full therapeutic potential. Here, we investigate the loading of a selective and potent anticancer drug, β-lapachone (β-lap), on a magnetite nanoparticle-decorated reduced graphene oxide ($Fe_3O_4$/rGO) and the *in vitro* anticancer efficacy of β-lap loaded $Fe_3O_4$/rGO. Reduced graphene oxide (rGO) with magnetic functionality was prepared via electrostatic interaction between positively charged magnetite ($Fe_3O_4$) nanoparticles and negatively charged GO, followed by hydrazine reduction of GO to rGO. The prepared $Fe_3O_4$/rGO shows that $Fe_3O_4$ makes the $Fe_3O_4$/rGO hybrid magnetically separable for easy handling during drug loading and release and the $Fe_3O_4$/rGO hybrid exhibits significantly higher loading capacity than that of $Fe_3O_4$/GO, suggesting that restoration of the graphene basal plane upon reduction of GO enhances the interaction between β-lap and rGO. Cellular uptake studies using fluorescently labeled $Fe_3O_4$/rGO verifies successful internalization of $Fe_3O_4$/rGO into the cytoplasm while rGO without hybridized $Fe_3O_4$ has poor uptake performance. Furthermore, β-lap loaded $Fe_3O_4$/rGO shows remarkably high cytotoxicity toward MCF-7 breast cancer cells while the blank $Fe_3O_4$/rGO produces no cytotoxic effects. The cytotoxicity results suggest that $Fe_3O_4$/rGO is an efficient drug carrier for anticancer treatments. The fine-tuning of the chemical structures of graphene oxides by reduction chemistry may provide a universal route for controlled loading and release of drugs or biomolecules to construct advanced delivery vehicles.

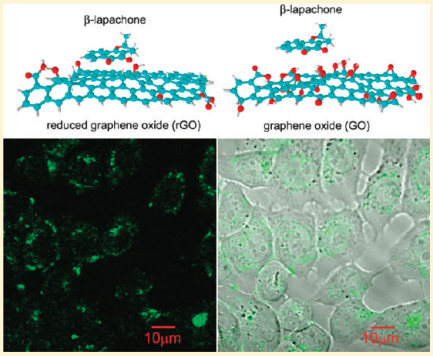


**KEYWORDS:** *β-lapachone, drug delivery, π−π stacking, reduced graphene oxide*

## INTRODUCTION

Drugs that exploit cancer-specific molecular targets have shown great promise to improve therapeutic efficiency while concurrently reducing toxic side effects.[1−6] Unlike most chemotherapeutic agents that are toxic to normal cells, β-lapachone (β-lap) is a potent antitumor agent that selectively kills NAD(P)H:quinone oxidoreductase-1 (NQO1) overexpressing cancer cells.[7,8] NQO1 is a flavoprotein overexpressed (up to 20-fold) in various human cancers, including those in lung, prostate, pancreas and breast;[2] nevertheless, the therapeutic applications have been hampered by its poor water solubility (0.038 mg $mL^{-1}$) and low bioavailability.[9] To solve these problems, β-lap is either complexed with cyclodextrin[9−11] or encapsulated inside a polymer micelle,[2] but the β-lap−cyclodextrin complex tends to dissociate very fast, leading to low tumor accumulation; furthermore, cyclodextrin causes many undesirable side effects such as cytotoxicity and severe hemolysis.[12] On the other hand, polymer micelles usually have very low β-lap loading capacity. It is critical to develop an efficient and biocompatible β-lap carrier to realize its full therapeutic potential.

Recently, the unique physiochemical properties of graphene oxide (GO)-based materials[13−17] have attracted enormous interest in various biomedical applications such as scaffolds,[18] biosensors,[19−23] imaging[24] and drug delivery.[25−28] In particular, its high specific surface area with a theoretical value of 2630 $m^2$ $g^{-1}$ renders it a promising drug carrier, and functionalized graphene oxides (GOs) have recently been explored as drug delivery vehicles for anticancer treatments.[25−30] Dai's group first employed PEGylated GO nanosheets to deliver hydrophobic anticancer drugs for high anticancer efficacy.[26,29] Chen and coworkers have also developed multifunctional GO nanocarriers for cell-targeted delivery of doxorubicin.[25,31] More recently, Zhang and colleagues have investigated the controlled loading and targeted delivery of mixed anticancer drugs using folic acid functionalized GO nanosheets.[28] Furthermore, the sequential delivery of a drug and a siRNA is also realized using polyethylenimine-functionalized GO to achieve an enhanced chemotherapeutic efficacy.[27] However, these drug delivery systems are mainly based on GO, and the applicability of reduced GO (rGO) in drug delivery has not been studied.

**Received:** October 18, 2011
**Revised:** January 11, 2012
**Accepted:** January 20, 2012
**Published:** January 20, 2012





dx.doi.org/10.1021/mp2005356 | *Mol. Pharmaceutics* 2012, 9, 615−621

We report here a magnetite nanoparticle-decorated reduced graphene oxide ($Fe_3O_4$/rGO) nanocarrier for high $\beta$-lap loading and efficient anticancer treatment. Magnetic $Fe_3O_4$ nanoparticles were first assembled onto GO nanosheets via electrostatic interaction, followed by controlled hydrazine reduction to rGO. The subsequent $\beta$-lap loading experiments compared the $\beta$-lap loading capacities of $Fe_3O_4$/rGO nanocarrier with the $Fe_3O_4$/GO counterpart. Finally, cell internalization study and *in vitro* cell cytotoxicity tests were performed to evaluate the anticancer efficacy of $\beta$-lap loaded $Fe_3O_4$/rGO.

## MATERIALS AND METHODS

**Chemicals.** $\beta$-Lapachone ($\beta$-lap) was obtained from Sigma (St. Louis, MO). The deionized water (18.2 MΩ·cm) was obtained from a Millipore Milli-Q water purification system. All other reagents were of analytical grade.

**Preparation and Characterization of Drug Nanocarriers.** Graphene oxide (GO) was prepared by a modified Hummer's method.[32,33] $Fe_3O_4$ nanoparticles were synthesized as reported.[34,35] In a typical process, the as-prepared $Fe_3O_4$ nanoparticles (50 mg) were dispersed into 100 mL of ethanol by ultrasonication. After 30 min, 1 mL of (3-aminopropyl)-triethoxysilane (APTES) was added to the solution and stirred for 2 h at room temperature to obtain APTES-modified $Fe_3O_4$ nanoparticles. Ten milliliters of APTES-modifed $Fe_3O_4$ nanoparticles (2.4 mg $mL^{-1}$) was then added into 50 mL of GO suspension (0.4 mg $mL^{-1}$) under magnetic stirring. After 1 h, the sample was magnetically collected and redispersed in 15 mL of water. 0.8 mL of hydrazine (65 wt %) was mixed with the above suspension overnight to reduce GO and finally obtain the $Fe_3O_4$/rGO nanocomposites.

The product morphology was examined by transmission electron microscope (TEM; JEOL, JEM-2100F, 200 kV) and field-emission scanning electron microscope (FESEM; JEOL, JSM-6700F, 5 kV). The amount of rGO present in the sample was determined by thermogravimetric analysis (TGA), which was carried out in a flow of air with a temperature ramp of 10 °C $min^{-1}$. Zeta potentials and hydrodynamic sizes were measured using a Zetasizer 3000 (Malvern Instruments). Fourier transform infrared spectroscopy (FTIR) spectra were obtained with a Perkin-Elmer FT-IR Spectrum GX.

**Determination of Drug Loading Capacity and *in Vitro* Release Study.** Aqueous $Fe_3O_4$/rGO suspension (0.4 mg $mL^{-1}$) was mixed with various concentrations of $\beta$-lap/DMSO solutions and stirred at room temperature. As a comparison, $Fe_3O_4$/GO was loaded with $\beta$-lap under similar conditions. At specified time points, the $\beta$-lap loaded sample was magnetically collected and the characteristic $\beta$-lap absorbance at 440 nm in the supernatant was measured using an UV−vis spectrophotometer. Loading capacity was calculated according to eq 1.

$$\text{drug loading capacity} = \frac{\text{mass of drug loaded}}{\text{mass of drug carrier}} \times 100\% \quad (1)$$

The release of $\beta$-lap from $Fe_3O_4$/rGO was tested in phosphate-buffered saline (PBS) or cell culture medium (10% FBS/DMEM) at 37 °C. The nanohybrids were magnetically collected and filtered every 24 h to measure the absorbance of the supernatant to estimate the released amount. The percentage of drug released was given by eq 2.

$$\text{percentage of drug released} = \frac{\text{mass of drug released}}{\text{mass of drug loaded}} \times 100\% \quad (2)$$

**Cell Culture.** MCF-7 cells were grown in Dulbecco's modified Eagle's medium (DMEM) (PAA Laboratories, Pasching, Austria) supplemented with 10% heat inactivated fetal bovine serum (FBS) (PAA laboratories), 1 mM L-glutamine (Gibco, Grand Island, NY) and 50 U $mL^{-1}$ penicillin/streptomycin (Gibco) in a humidified incubator with 5.0% $CO_2$ at 37 °C.

**Cellular Uptake.** The nanohydrid was first fluorescently labeled by mixing 0.5 mL of fluorescein isothiocyanate (FITC) (0.1 mg $mL^{-1}$) and 2 mL of $Fe_3O_4$/rGO (1 mg $mL^{-1}$) overnight. The FITC labeled $Fe_3O_4$/rGO was centrifuged and washed 3 times. The MCF-7 cells were incubated with 10 $\mu$g $mL^{-1}$ FITC labeled sample at 37 °C for 2 h. After rinsing, the cells were examined using a confocal laser scanning microscope (CLSM) (LSM 510 META, Carl Zeiss, Germany).

**Cytotoxicity Assay.** The viability and proliferation of cells were evaluated using 3-[4,5-dimethylthiazol-2-yl]-2,5-diphenyltetrazolium bromide (MTT) assay. The MTT assay was performed in triplicate as reported.[36] Briefly, MCF-7 cells were seeded into 96-well plates at a density of $1 \times 10^4$ per well in 200 $\mu$L of medium and grown overnight. The cells were then incubated with various concentrations of free $\beta$-lap, $\beta$-lap free $Fe_3O_4$/rGO or $\beta$-lap loaded sample for 4 h. Following this incubation, cells were incubated in medium containing 0.5 mg $mL^{-1}$ of MTT for 4 h. Thereafter, the MTT solution was removed and the precipitated violet crystals were dissolved in 200 $\mu$L of DMSO. The absorbance at 570 nm was measured using a BioTek microplate reader.

## RESULTS AND DISCUSSION

**Characterization of the $Fe_3O_4$/rGO Nanohybrids.** Uniform magnetic $Fe_3O_4$ nanoparticles were first functionalized with APTES to generate amine groups and subsequently attached to the GO nanosheets. GO can bind to the $NH_2$ groups generated on the $Fe_3O_4$ nanoparticle surfaces through hydrogen bonds. The measured zeta potentials of $NH_2$ functionalized $Fe_3O_4$ nanoparticles and GO are 27.3 ± 3.94 mV and −48.5 ± 8.69 mV, respectively, thus indicating that electrostatic interactions also contribute to the formation of $Fe_3O_4$/GO. Then the $Fe_3O_4$/GO nanohybrids were reduced by hydrazine treatment to produce $Fe_3O_4$/rGO. The measured zeta potential of rGO is −45.3 ± 13.8 mV (Figure S1 in the Supporting Information), showing that the $Fe_3O_4$ nanoparticles remain attached to rGO by electrostatic interactions. The $Fe_3O_4$/rGO nanohybrid is magnetically separable as shown in Figure S2 in the Supporting Information, which allows easy handling during drug loading and release. In the latter sections, the compositions and drug loading capacities of $Fe_3O_4$/GO and $Fe_3O_4$/rGO are compared to determine the more efficient drug carrier.

The morphology of the $Fe_3O_4$/rGO nanohybrid characterized by FESEM in Figure 1a,b clearly illustrates that $Fe_3O_4$ nanoclusters of only tens of nanometers in size are uniformly distributed on the surfaces of rGOs. The rGO supports can be easily identified as wrinkle-like structures (Figure 1b). The TEM images (Figure 1c,d) confirm that rGO sheets are decorated with clusters of $Fe_3O_4$ nanoparticles with sizes less than 20 nm. These attached $Fe_3O_4$ nanoparticles could be


dx.doi.org/10.1021/mp2005356 | Mol. Pharmaceutics 2012, 9, 615−621

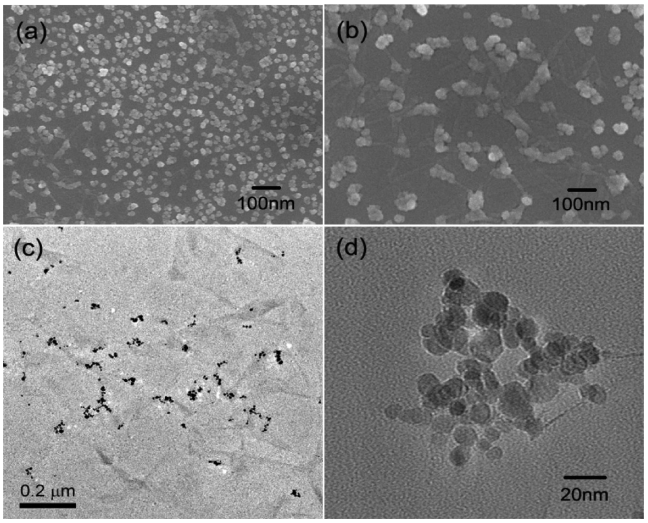


**Figure 1.** (a) Low magnification and (b) high magnification field-emission scanning electron microscope (FESEM) images; (c) low magnification and (d) high magnification transmission electron microscope (TEM) images of $Fe_3O_4$/rGO used for $\beta$-lap loading.

potentially used for magnetically targeted drug delivery while acting as a contrast agent for MRI imaging. The slight agglomeration of the nanoparticles observed in Figure 1d could probably be caused by the folding of the rGO substrate. It is worthy of note that the hydrodynamic size of the nanohybrid is ~130 nm (Figure 2b), which is suitable for cell internalization and prolonged circulation.[37] Meanwhile, its zeta potential is approximately −43.3 mV (Figure 2a), verifying its ability to form a stable colloidal solution (Figure 4a, inset).

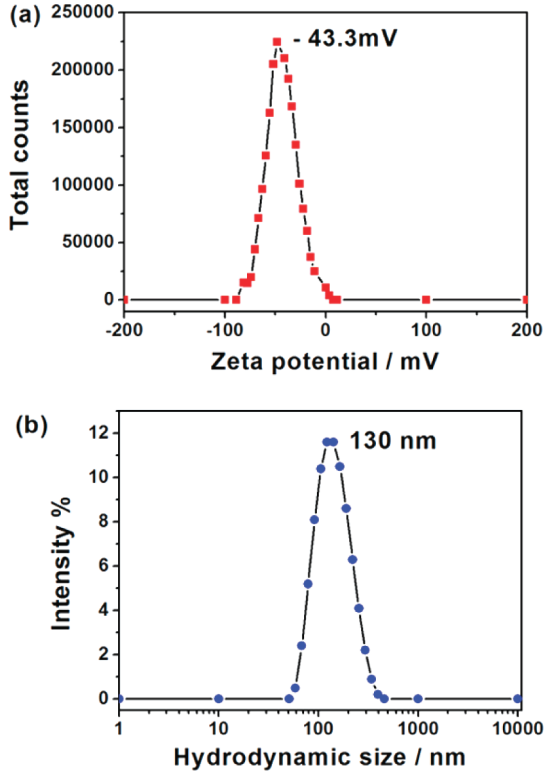


**Figure 2.** The (a) hydrodyanmic size and (b) zeta potential distribution of the sample.

The nanohybrids were examined by FTIR (Figure 3a). Both $Fe_3O_4$/rGO and $Fe_3O_4$/GO show a peak at 569 $cm^{-1}$, which corresponds to the stretching vibration of Fe−O bond in pure $Fe_3O_4$ (Figure S3 in the Supporting Information),[31,38] verifying the presence of $Fe_3O_4$ nanoparticles in the nanohybrids. The existence of C═O (1723 $cm^{-1}$), C═C (1590 $cm^{-1}$), and C−O (1042 $cm^{-1}$) functional groups[29] is confirmed in $Fe_3O_4$/GO, whereas for $Fe_3O_4$/rGO, the peak at 1723 $cm^{-1}$ diminishes, indicating the successful reduction by hydrazine. The weight fraction of the carbonaceous support in $Fe_3O_4$/GO and $Fe_3O_4$/rGO was determined by TGA (Figure 3b). For $Fe_3O_4$/GO, two stages of weight loss occur at around ~220 °C and ~475 °C. The mass loss at ~220 °C is presumably due to pyrolysis of the labile oxygen-containing functional groups.[39,40] On the other hand, only a single large weight loss can be observed at ~500 °C for $Fe_3O_4$/rGO, which is attributed to the bulk pyrolysis of the carbon skeleton.[40] The respective GO and rGO contents in $Fe_3O_4$/GO and $Fe_3O_4$/rGO nanohybrids are 46 wt % and 49 wt %, respectively.

**Drug Loading.** $\beta$-Lap was then loaded onto the surface of the nanohybrids via a simple mixing and sonication method. The unbound drug was removed by magnetic separation, and the loading capacity of $\beta$-lap on nanohybrids was calculated by measuring the concentration of unbound $\beta$-lap using UV−vis spectra. As shown in Figure 4a, the loading of $\beta$-lap takes place rapidly in the first 2 h for $Fe_3O_4$/rGO and is followed by a slower loading rate to reach a plateau at around 24 h. The saturated $\beta$-lap loading capacity on $Fe_3O_4$/rGO is 46% with an initial $\beta$-lap concentration of 0.4 mg $mL^{-1}$, considerably higher than the previously reported values.[2] In contrast, $Fe_3O_4$/GO shows no significant $\beta$-lap loading, proving that rGO is responsible for large $\beta$-lap loading. The loading capacities of $Fe_3O_4$ and rGO are also presented for comparison in Figure 5a, which clearly shows that $Fe_3O_4$ nanoparticles demonstrate almost no ability for $\beta$-lap loading, whereas rGO has a loading capacity of 83%, nearly 2 times that of $Fe_3O_4$/rGO. This is understandable since the rGO content in the $Fe_3O_4$/rGO nanohybrid is 49 wt %. The above results suggest that the reduced chemical state of rGO is the main cause for the much higher loading capacity of $\beta$-lap. The effect of the hydrazine reduction time on the $\beta$-lap loading capacity of $Fe_3O_4$/rGO was investigated. The result in Figure 5b shows that the loading capacity increases with the reduction time until achieving the maximum loading capacity after an 8 h reduction. Further increasing the reduction time does not lead to a significant enhancement in loading capacity.

We argue that the contrasting $\beta$-lap loading capacities of $Fe_3O_4$/rGO and $Fe_3O_4$/GO are due to the different chemical structures of rGO versus GO for significantly different strengths of $\pi-\pi$ stacking and hydrophobic interactions with $\beta$-lap. GO possesses plenty of functional groups, of which epoxies (−O−) and hydroxyls (−OH) are located on the basal planes whereas carbonyls (−C═O) and carboxyls (−COOH) are mainly distributed at the edges;[42] thus, GO consists of ordered small (2−3 nm) $sp^2$ clusters isolated within the $sp^3$ C−O matrix (Figure 4c). Upon reduction of GO, most oxygen-containing groups are removed to create new $sp^2$ clusters and at the same time restore a planar structure[14] as illustrated in Figure 4d. Because of the increased amount of $sp^2$ structural domains, rGO has a very high tendency to bind with neutral and aromatic $\beta$-lap molecules via favorable $\pi-\pi$ stacking and hydrophobic interactions. However, the interaction between $\beta$-lap and hydrophilic GO is considerably weaker, leading to the insignificant loading capacity of GO.


dx.doi.org/10.1021/mp2005356 | Mol. Pharmaceutics 2012, 9, 615−621

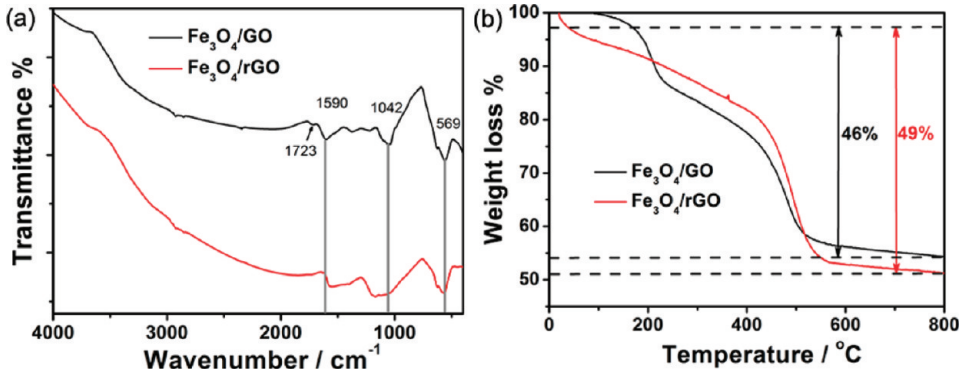


**Figure 3.** (a) Fourier transform infrared spectroscopy (FTIR) spectra and (b) thermal gravimetric analysis (TGA) of $Fe_3O_4$/GO and $Fe_3O_4$/rGO.

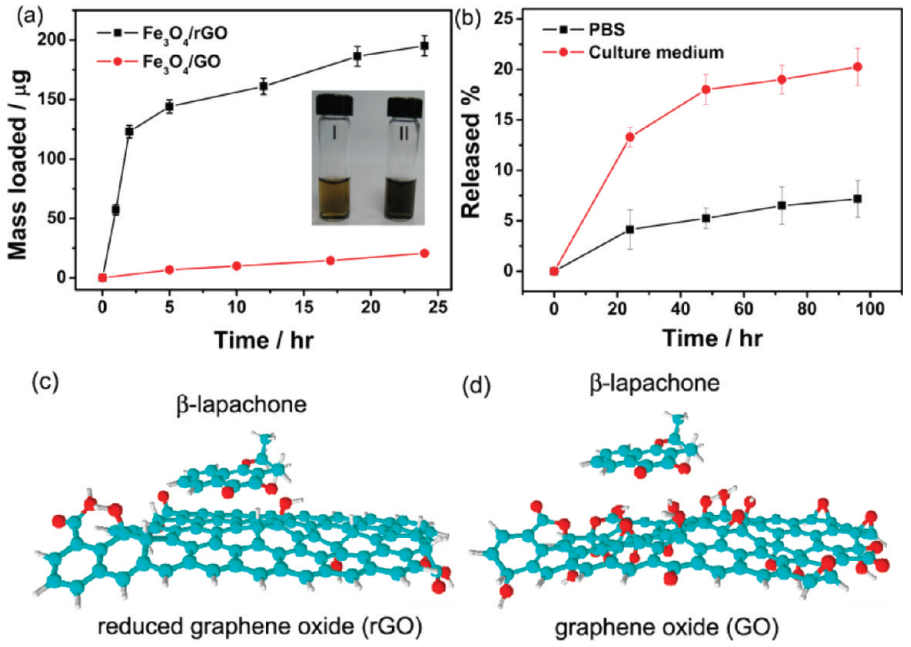


**Figure 4.** (a) Loading of $\beta$-lap onto the $Fe_3O_4$/rGO as compared to $Fe_3O_4$/GO with respect to time. Inset shows the photos of the stable aqueous solutions formed by $Fe_3O_4$/GO (I) and $Fe_3O_4$/rGO (II). (b) Release profile of $\beta$-lap from $Fe_3O_4$/rGO in PBS vs cell culture medium. (c, d) Schematics illustrating the differential loading of $\beta$-lap onto (c) rGO and (d) GO at atomic level according to the modified Lerf–Klinowski model proposed by Gao et al.[41]

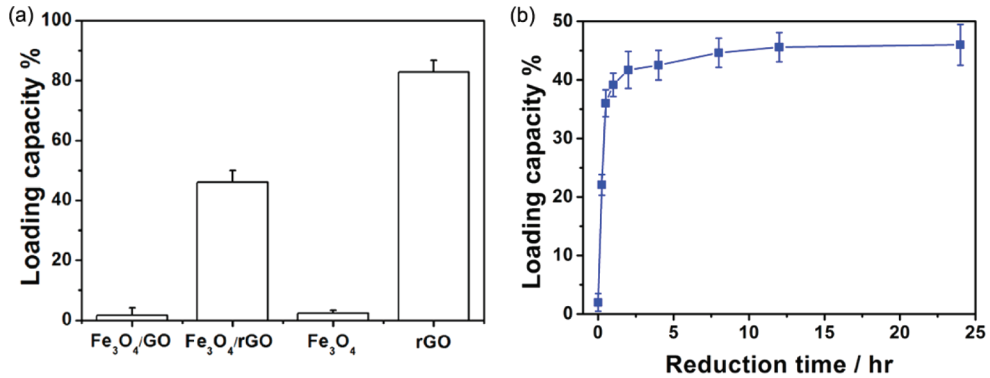


**Figure 5.** (a) Comparison of the $\beta$-lap loading capacity of different drug carriers. (b) The effect of increasing reduction time on the $\beta$-lap loading capacity.

***In Vitro* Drug Release.** The $\beta$-lap release kinetics was investigated in phosphate buffer saline (PBS) and cell culture medium (10% FBS/DMEM). As shown in Figure 4b, the $\beta$-lap release is negligible in PBS whereas ~20% is released in cell culture medium after a 4 day incubation. Similar drug release profiles have been observed for previously reported GO or


dx.doi.org/10.1021/mp2005356 | *Mol. Pharmaceutics* 2012, 9, 615–621

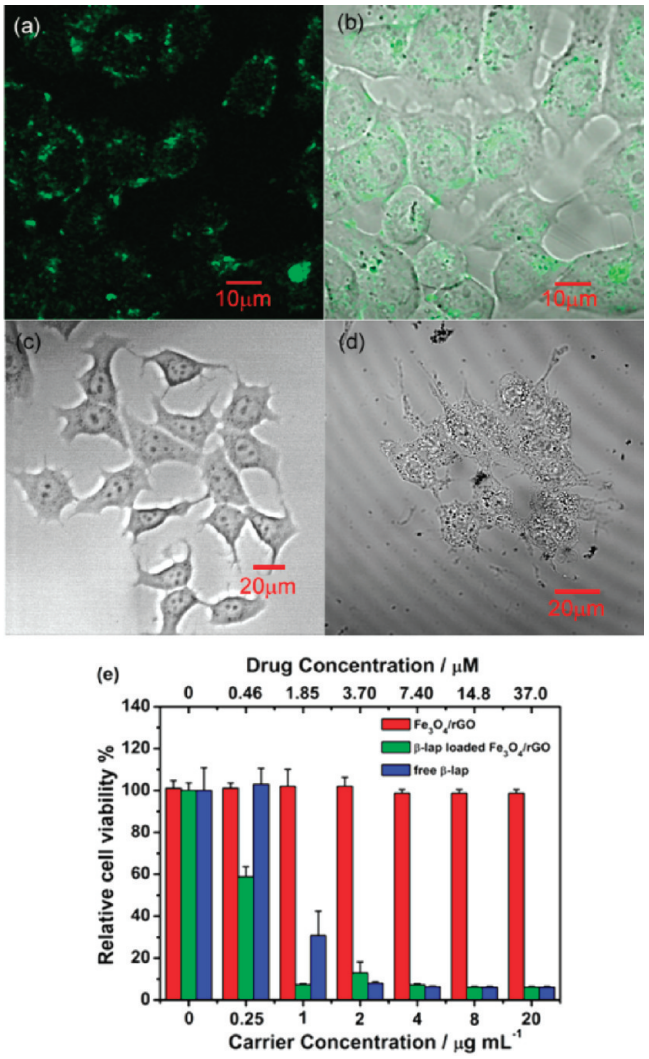


**Figure 6.** (a) Fluorescence image and (b) merged fluorescence and bright-field image showing the cellular uptake of FITC-labeled $Fe_3O_4$/rGO after 2 h incubation at 37 °C. (c, d) Bright-field images showing the morphologies of MCF-7 cells after incubation with (c) blank $Fe_3O_4$/rGO and (d) $\beta$-lap loaded $Fe_3O_4$/rGO. (e) *In vitro* cell toxicity assay results showing the relative cell viability (vs untreated control) of MCF-7 cells incubated with blank $Fe_3O_4$/rGO, $\beta$-lap loaded $Fe_3O_4$/rGO and free $\beta$-lap at different concentrations for 4 h.

multiwalled carbon nanotube (MWCNT)-based drug carriers.[26,28] The release profile confirms the stability of $\beta$-lap on $Fe_3O_4$/rGO, suggesting that it can be protected in the bloodstream before reaching the targeted tumor site. The slow release behavior is very different from that of reported polymer based drug delivery systems where the time for 50% of $\beta$-lap release is 18 h and even over 4 days for ~75% release.[2] This indicates a stronger interaction between $\beta$-lap and $Fe_3O_4$/rGO. We note a higher $\beta$-lap release efficiency in culture medium with 10% serum as compared to that in PBS, and this is likely due to the preferential binding of $\beta$-lap molecules with serum proteins.[26] Since the cell interior contains even more organic compounds such as proteins, lipids and complex sugars,[43,44] it is expected that the release of $\beta$-lap from the nanocarrier is even faster after cellular uptake to achieve a sufficient intracellular delivery. The fine-tuning of the chemical structures of graphene oxides by reduction chemistry may provide a route to delicately adjust drug loading and release.

**Cellular Uptake and *in Vitro* Cytotoxicity.** Cellular uptake of $Fe_3O_4$/rGO was examined by confocal laser scanning microscopy (CLSM) after 2 h incubation with the cells. Green fluorescence of FITC-labeled $Fe_3O_4$/rGO observed in the cytoplasm (Figure 6a,b) proves the successful internalization of $Fe_3O_4$/rGO. The cellular internalizations of FITC-labeled $Fe_3O_4$ nanoparticles and rGO were investigated as shown in Figure S4 in the Supporting Information for comparison. Although $Fe_3O_4$ nanoparticles can be internalized into the cytoplasm, they are heavily aggregated to form microsized agglomerations which could severely hinder the intracellular release of drug and trafficking of drug molecules to the target sites. In contrast, the cellular uptake of bare rGO is almost negligible, and thus it cannot be applied alone for intracellular delivery. These results clearly indicate that $Fe_3O_4$ nanoparticles attached on rGO enhance the cellular uptake while stabilizing the $Fe_3O_4$ by anchoring on rGO support to maintain a monodispersed state without agglomeration. Considering both the drug loading capacity and the cellular uptake efficiency, the $Fe_3O_4$/rGO nanohybrid is certainly a better drug delivery system in comparison to individual $Fe_3O_4$ and rGO components.

We then evaluated the anticancer efficacy of $\beta$-lap loaded $Fe_3O_4$/rGO using the MCF-7 breast cancer cell line. Comparing Figure 6c,d, obvious morphological change such as cell shrinkage can be observed after the MCF-7 cells are incubated with $\beta$-lap loaded $Fe_3O_4$/rGO for 4 h. The MTT assay result indicates that the $\beta$-lap loaded $Fe_3O_4$/rGO is highly potent to kill MCF-7 cells (Figure 6e). The 50% growth inhibition concentration (IC50) for $\beta$-lap loaded $Fe_3O_4$/rGO is approximately 0.5 $\mu$M, which is even lower than that of free $\beta$-lap (~1.5 $\mu$M). It is worthy of note that no obvious toxicity is found for various concentrations of $Fe_3O_4$/rGO without $\beta$-lap loading, indicating the biocompatible nature of the drug carrier. These results demonstrate that $Fe_3O_4$/rGO is a very efficient drug delivery vehicle.

## ■ CONCLUSIONS

In summary, we have utilized a magnetically functionalized rGO with good biocompatibility for the intracellular delivery of an anticancer drug, $\beta$-lap, that is very hard to be carried by other delivery vehicles. We discover that, after restoring the planar structure of rGO via chemical reduction, the $Fe_3O_4$/rGO exhibits a much higher $\beta$-lap loading capacity than its $Fe_3O_4$/GO counterpart. A mechanism based on the unique chemical structure with restored basal planes of rGO from GO is proposed to explain the large $\beta$-lap loading capacity. Cellular uptake studies using fluorescently labeled $Fe_3O_4$/rGO and its components indicate that $Fe_3O_4$ in the hybrid plays a critical role in more efficient internalization of $Fe_3O_4$/rGO into the cytoplasm. It is also demonstrated that $\beta$-lap loaded $Fe_3O_4$/rGO has remarkably high cytotoxicity toward MCF-7 breast cancer cells while the blank $Fe_3O_4$/rGO produces no cytotoxic effects, demonstrating its potential as a highly efficient drug delivery vehicle. The fine-tuning of the chemical structures of graphene oxides by reduction chemistry can be further explored as a versatile route for controlled loading and release of drugs or other biomolecules. In addition, $Fe_3O_4$ nanoparticles allow the hybrid to be potentially applicable in magnetic targeting and magnetic resonance imaging (MRI),[45] and the work will be conducted in our lab.


dx.doi.org/10.1021/mp2005356 | *Mol. Pharmaceutics* 2012, 9, 615–621

## ■ ASSOCIATED CONTENT

### Supporting Information

Additional figures as discussed in the text. This material is available free of charge via the Internet at http://pubs.acs.org.

## ■ AUTHOR INFORMATION


### Corresponding Author

*Nanyang Technological University, School of Chemical and Biomedical Engineering, 70 Nanyang Drive, Singapore 637457, Singapore. Tel: +65 67904485. Fax: +65 67911761. E-mail: ecmli@ntu.edu.sg.


### Notes

The authors declare no competing financial interest.

## ■ ACKNOWLEDGMENTS

This work is financially supported by Institute for Clean Energy and Advanced Materials, Southwest University, Chongqing, China and Center of Advanced Bionanosystems of Nanyang Technological University in Singapore.

## ■ REFERENCES


(1) Ai, S. B.; Duan, J. L.; Liu, X.; Bock, S.; Tian, Y. A.; Huang, Z. B. Biological Evaluation of a Novel Doxorubicin-Peptide Conjugate for Targeted Delivery to EGF Receptor-Overexpressing Tumor Cells. *Mol. Pharmaceutics* **2011**, *8* (2), 375−386.

(2) Blanco, E.; Bey, E. A.; Dong, Y.; Weinberg, B. D.; Sutton, D. M.; Boothman, D. A.; Gao, J. M. beta-Lapachone-containing PEG-PLA polymer micelles as novel nanotherapeutics against NQO1-overexpres sing tumor cells. *J. Controlled Release* **2007**, *122* (3), 365−374.

(3) Wang, J. Z.; Zhong, C.; Wexler, D.; Idris, N. H.; Wang, Z. X.; Chen, L. Q.; Liu, H. K. Graphene-Encapsulated Fe3O4 Nanoparticles with 3D Laminated Structure as Superior Anode in Lithium Ion Batteries. *Chem.—Eur. J.* **2011**, *17* (2), 661−667.

(4) Aina, O. H.; Liu, R. W.; Sutcliffe, J. L.; Marik, J.; Pan, C. X.; Lam, K. S. From combinatorial chemistry to cancer-targeting peptides. *Mol. Pharmaceutics* **2007**, *4* (5), 631−651.

(5) Platt, V. M.; Szoka, F. C. Anticancer therapeutics: Targeting macromolecules and nanocarriers to hyaluronan or CD44, a hyaluronan receptor. *Mol. Pharmaceutics* **2008**, *5* (4), 474−486.

(6) Tai, W. Y.; Shukla, R. S.; Qin, B.; Li, B. Y.; Cheng, K. Development of a Peptide-Drug Conjugate for Prostate Cancer Therapy. *Mol. Pharmaceutics* **2011**, *8* (3), 901−912.

(7) Bey, E. A.; Bentle, M. S.; Reinicke, K. E.; Dong, Y.; Yang, C. R.; Girard, L.; Minna, J. D.; Bornmann, W. G.; Gao, J. M.; Boothman, D. A. An NQO1-and PARP-1-mediated cell death pathway induced in non-small-cell lung cancer cells by beta-lapachone. *Proc. Natl. Acad. Sci. U.S.A.* **2007**, *104* (28), 11832−11837.

(8) Li, Y. Z.; Sun, X. G.; LaMont, J. T.; Pardee, A. B.; Li, C. J. Selective killing of cancer cells by beta-lapachone: Direct checkpoint activation as a strategy against cancer. *Proc. Natl. Acad. Sci. U.S.A.* **2003**, *100* (5), 2674−2678.

(9) Nasongkla, N.; Wiedmann, A. F.; Bruening, A.; Beman, M.; Ray, D.; Bornmann, W. G.; Boothman, D. A.; Gao, J. M. Enhancement of solubility and bioavailability of beta-lapachone using cyclodextrin inclusion complexes. *Pharm. Res.* **2003**, *20* (10), 1626−1633.

(10) Park, C.; Youn, H.; Kim, H.; Noh, T.; Kook, Y. H.; Oh, E. T.; Park, H. J.; Kim, C. Cyclodextrin-covered gold nanoparticles for targeted delivery of an anti-cancer drug. *J. Mater. Chem.* **2009**, *19* (16), 2310−2315.

(11) Jeong, S. Y.; Park, S. J.; Yoon, S. M.; Jung, J.; Woo, H. N.; Yi, S. L.; Song, S. Y.; Park, H. J.; Kim, C.; Lee, J. S.; Choi, E. K. Systemic delivery and preclinical evaluation of Au nanoparticle containing beta-lapachone for radiosensitization. *J. Controlled Release* **2009**, *139* (3), 239−245.

(12) Blanchemain, N.; Karrout, Y.; Tabary, N.; Neut, C.; Bria, M.; Siepmann, J.; Hildebrand, H. F.; Martel, B. Methyl-beta-cyclodextrin modified vascular prosthesis: Influence of the modification level on the drug delivery properties in different media. *Acta Biomater.* **2011**, *7* (1), 304−314.

(13) Allen, M. J.; Tung, V. C.; Kaner, R. B. Honeycomb Carbon: A Review of Graphene. *Chem. Rev.* **2010**, *110* (1), 132−145.

(14) Loh, K. P.; Bao, Q. L.; Eda, G.; Chhowalla, M. Graphene oxide as a chemically tunable platform for optical applications. *Nat. Chem.* **2010**, *2* (12), 1015−1024.

(15) Geim, A. K.; Novoselov, K. S. The rise of graphene. *Nat. Mater.* **2007**, *6* (3), 183−191.

(16) Rao, C. N. R.; Sood, A. K.; Subrahmanyam, K. S.; Govindaraj, A. Graphene: The New Two-Dimensional Nanomaterial. *Angew. Chem., Int. Ed.* **2009**, *48* (42), 7752−7777.

(17) Guo, C. X.; Yang, H. B.; Sheng, Z. M.; Lu, Z. S.; Song, Q. L.; Li, C. M. Layered Graphene/Quantum Dots for Photovoltaic Devices. *Angew. Chem., Int. Ed.* **2010**, *49* (17), 3014−3017.

(18) Depan, D.; Girase, B.; Shah, J. S.; Misra, R. D. K. Structure-process-property relationship of the polar graphene oxide-mediated cellular response and stimulated growth of osteoblasts on hybrid chitosan network structure nanocomposite scaffolds. *Acta Biomater.* **2011**, *7* (9), 3432−3445.

(19) Hu, Y.; Li, F.; Bai, X.; Li, D.; Hua, S.; Wang, K.; Niu, L. Label-free electrochemical impedance sensing of DNA hybridization based on functionalized graphene sheets. *Chem. Commun.* **2011**, *47* (6), 1743−1745.

(20) Zhang, X.; Li, S.; Jin, X.; Zhang, S. A new photoelectrochemical aptasensor for the detection of thrombin based on functionalized graphene and CdSe nanoparticles multilayers. *Chem. Commun.* **2011**, *47* (17), 4929−4931.

(21) Liu, M.; Zhao, H.; Quan, X.; Chen, S.; Fan, X. Distance-independent quenching of quantum dots by nanoscale-graphene in self-assembled sandwich immunoassay. *Chem. Commun.* **2010**, *46* (42), 7909−7911.

(22) Guo, C. X.; Zheng, X. T.; Lu, Z. S.; Lou, X. W.; Li, C. M. Biointerface by Cell Growth on Layered Graphene−Artificial Peroxidase−Protein Nanostructure for In Situ Quantitative Molecular Detection. *Adv. Mater.* **2010**, *22* (45), 5164−5167.

(23) Zheng, X. T.; Li, C. M. Single cell analysis at the nanoscale. *Chem. Soc. Rev.* **2011**, DOI: 10.1039/C1CS15265C .

(24) Peng, C.; Hu, W. B.; Zhou, Y. T.; Fan, C. H.; Huang, Q. Intracellular Imaging with a Graphene-Based Fluorescent Probe. *Small* **2010**, *6* (15), 1686−1692.

(25) Yang, X. Y.; Wang, Y. S.; Huang, X.; Ma, Y. F.; Huang, Y.; Yang, R. C.; Duan, H. Q.; Chen, Y. S. Multi-functionalized graphene oxide based anticancer drug-carrier with dual-targeting function and pH-sensitivity. *J. Mater. Chem.* **2011**, *21* (10), 3448−3454.

(26) Liu, Z.; Robinson, J. T.; Sun, X. M.; Dai, H. J. PEGylated nanographene oxide for delivery of water-insoluble cancer drugs. *J. Am. Chem. Soc.* **2008**, *130* (33), 10876−10877.

(27) Zhang, L. M.; Lu, Z. X.; Zhao, Q. H.; Huang, J.; Shen, H.; Zhang, Z. J. Enhanced Chemotherapy Efficacy by Sequential Delivery of siRNA and Anticancer Drugs Using PEI-Grafted Graphene Oxide. *Small* **2011**, *7* (4), 460−464.

(28) Zhang, Y. B.; Ali, S. F.; Dervishi, E.; Xu, Y.; Li, Z. R.; Casciano, D.; Biris, A. S. Cytotoxicity Effects of Graphene and Single-Wall Carbon Nanotubes in Neural Phaeochromocytoma-Derived PC12 Cells. *ACS Nano* **2010**, *4* (6), 3181−3186.

(29) Sun, X. M.; Liu, Z.; Welsher, K.; Robinson, J. T.; Goodwin, A.; Zaric, S.; Dai, H. J. Nano-Graphene Oxide for Cellular Imaging and Drug Delivery. *Nano Res.* **2008**, *1* (3), 203−212.

(30) Yuan, W. Y.; Li, C. M. Exponentially growing layer-by-layer assembly to fabricate pH-responsive hierarchical nanoporous polymeric film and its superior controlled release performance. *Chem. Commun.* **2010**, *46* (48), 9161−9163.

(31) Yang, X. Y.; Zhang, X. Y.; Ma, Y. F.; Huang, Y.; Wang, Y. S.; Chen, Y. S. Superparamagnetic graphene oxide-$Fe_3O_4$ nanoparticles hybrid for controlled targeted drug carriers. *J. Mater. Chem.* **2009**, *19* (18), 2710−2714.

(32) Hummers, W. S.; Offeman, R. E. Preparation of graphitic oxide. *J. Am. Chem. Soc.* **1958**, *80* (6), 1339−1339.
(33) Liang, Y. Y.; Wang, H. L.; Casalongue, H. S.; Chen, Z.; Dai, H. J. TiO2 Nanocrystals Grown on Graphene as Advanced Photocatalytic Hybrid Materials. *Nano Res.* **2010**, *3* (10), 701−705.
(34) Sahoo, Y.; Goodarzi, A.; Swihart, M. T.; Ohulchanskyy, T. Y.; Kaur, N.; Furlani, E. P.; Prasad, P. N. Aqueous ferrofluid of magnetite nanoparticles: Fluorescence labeling and magnetophoretic control. *J. Phys. Chem. B* **2005**, *109* (9), 3879−3885.
(35) Hu, Y.; Zheng, X. T.; Chen, J. S.; Zhou, M. J.; Li, C. M.; Lou, X. W. Silica-based complex nanorattles as multifunctional carrier for anticancer drug. *J. Mater. Chem.* **2011**, *21* (22), 8052−8056.
(36) Lu, Z. S.; Zhu, Z. H.; Zheng, X. T.; Qiao, Y.; Guo, J.; Li, C. M. Biocompatible fluorescence-enhanced $ZrO_2$-CdTe quantum dot nanocomposite for in vitro cell imaging. *Nanotechnology* **2011**, DOI: 10.1088/0957-4484/22/15/155604.
(37) Petros, R. A.; DeSimone, J. M. Strategies in the design of nanoparticles for therapeutic applications. *Nat. Rev. Drug Discovery* **2010**, *9* (8), 615−627.
(38) Zhang, J.; Rana, S.; Srivastava, R. S.; Misra, R. D. K. On the chemical synthesis and drug delivery response of folate receptor-activated, polyethylene glycol-functionalized magnetite nanoparticles. *Acta Biomater.* **2008**, *4* (1), 40−48.
(39) Shen, J. F.; Hu, Y. H.; Li, C.; Qin, C.; Ye, M. X. Synthesis of Amphiphilic Graphene Nanoplatelets. *Small* **2009**, *5* (1), 82−85.
(40) Zhu, C. Z.; Guo, S. J.; Fang, Y. X.; Dong, S. J. Reducing Sugar: New Functional Molecules for the Green Synthesis of Graphene Nanosheets. *ACS Nano* **2010**, *4* (4), 2429−2437.
(41) Gao, W.; Alemany, L. B.; Ci, L. J.; Ajayan, P. M. New insights into the structure and reduction of graphite oxide. *Nat. Chem.* **2009**, *1* (5), 403−408.
(42) Gao, X. F.; Jang, J.; Nagase, S. Hydrazine and Thermal Reduction of Graphene Oxide: Reaction Mechanisms, Product Structures, and Reaction Design. *J. Phys. Chem. C* **2010**, *114* (2), 832−842.
(43) Ellis, R. J.; Minton, A. P. Cell biology—Join the crowd. *Nature* **2003**, *425* (6953), 27−28.
(44) Liu, K. P.; Zhang, J. J.; Cheng, F. F.; Zheng, T. T.; Wang, C. M.; Zhu, J. J. Green and facile synthesis of highly biocompatible graphene nanosheets and its application for cellular imaging and drug delivery. *J. Mater. Chem.* **2011**, *21* (32), 12034−12040.
(45) Laurent, S.; Forge, D.; Port, M.; Roch, A.; Robic, C.; Elst, L. V.; Muller, R. N. Magnetic iron oxide nanoparticles: Synthesis, stabilization, vectorization, physicochemical characterizations, and biological applications. *Chem. Rev.* **2008**, *108* (6), 2064−2110.